



# Electrospinning of photo-responsive Azo-Cellulose: towards smart fibrous materials

Issei Otsuka · Christopher J. Barrett

Received: 9 April 2019 / Accepted: 19 June 2019 / Published online: 25 June 2019  
© Springer Nature B.V. 2019

**Abstract** Fabrication of nano/micro fibers of a photo-responsive cellulose derivative via electrospinning is demonstrated for the first time. Commercially available microcrystalline cellulose (Avicel®) is functionalized with a reversible molecular photo-switch, azobenzene, via esterification between the hydroxyl groups of cellulose and 4-(phenylazo)benzoyl chloride in anhydrous pyridine. The obtained azobenzene-functionalized cellulose (Azo-Cel) is soluble in several organic solvents that are commonly used for electrospinning, such as dichloromethane (DCM), tetrahydrofuran (THF), and *N,N*-dimethylformamide

(DMF). UV-Vis absorption spectral analysis of Azo-Cel solutions confirm successful reversible *cis/trans* isomerization of the azobenzene moiety via photo-irradiation and thermal relaxation. The electrospinning of Azo-Cel solutions in high-volatile DCM, low-volatile DMF, and their mixtures is investigated. The morphology of the electrospun products characterized by scanning electron microscopy varies from porous/non-porous fibers to irregular spherical beads, depending on the volatility of the solvent.

---

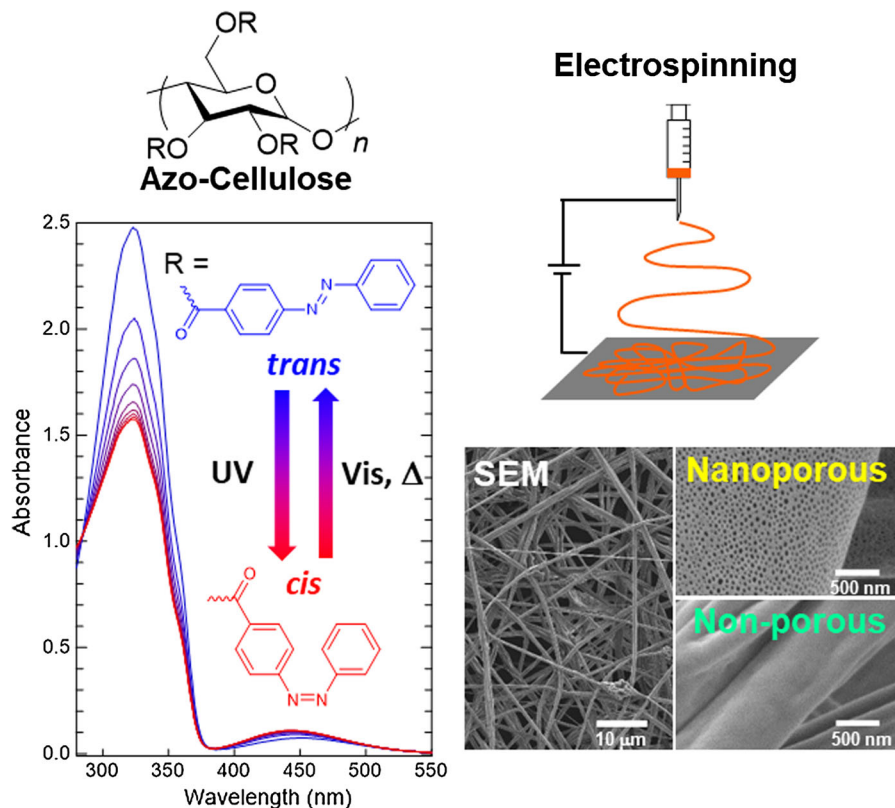
**Electronic supplementary material** The online version of this article (<https://doi.org/10.1007/s10570-019-02585-9>) contains supplementary material, which is available to authorized users.

---

I. Otsuka (✉)  
CNRS, CERMAV, Université Grenoble Alpes,  
38000 Grenoble, France  
e-mail: issei.otsuka@cermav.cnrs.fr

C. J. Barrett  
Department of Chemistry, McGill University,  
Montreal H3A 0B8, Canada  
e-mail: chris.barrett@mcgill.ca

## Graphic abstract



**Keywords** Cellulose · Azobenzene · Electrospinning · Nano/micro fibers · Photo-responsive materials

## Introduction

There are continued opportunities for the effective utilization of biomass towards functional materials, motivated by both a reduction of environmental burden, and access to the superior mechanical properties offered by bio-sourced polymers. Polysaccharides in particular, represented by cellulose, are one of the most abundant raw materials derived from biomass and renewable resources from forestry. The spotlight has been on not only their potential as alternatives for petrochemicals, but also their superior properties as biocompatible, biodegradable, and bioactive natural materials (Klemm et al. 2005). Cellulose-based materials are also well-suited for development of stimuli-

responsive polymers, which have received intense recent study since the behavior of these polymers can be controlled by simple changes of their surrounding media. Among the wide variety of stimuli-responsive polymers, photo-responsive polymers in particular have recently attracted much attention (Ercole et al. 2010) since the stimulus (light) can be precisely localized in time and space, and can also be triggered remotely from outside the system. Because of a large previous scientific gap between glycoscience and photo-science, these two research fields have not overlapped deeply yet, and thus there is a great potential with new materials such as nanocellulose-dye conjugates (Chauhan et al. 2014; Dong and Roman 2007; Gorgieva et al. 2015; Huang et al. 2013; Nielsen et al. 2010) engineered from the cross-domains of these research fields. Almost all of the recent reports on photo-reversible materials, as photo-actuators or “artificial muscles”, employ either soft Liquid Crystal Elastomers (LCEs) (Ikeda et al. 2007; Pei et al. 2014; Zeng et al. 2018) or gels (Harada et al.

2014; Ikejiri et al. 2018), both host materials suffering from fundamental limitations of fragility. In the mid- to late-1980s, some initial strong and robust cellulose derivatives combined with a reversible molecular photo-switch, azobenzene, as their pendant groups were prepared for a potential application as a switchable stationary phase for high-performance liquid chromatography (HPLC) (Okamoto et al. 1986) and thin layer chromatography (TLC) (Arai and Udagawa 1988). The *cis/trans* geometric photoisomerization of the azobenzene moiety changed the efficiency of resolution of the analyte, which was attributed to a higher-ordered geometric structure of the *trans*-isomer due to its liquid-crystalline nature, than the less-ordered structure of the *cis*-isomer. Since these early preliminary reports published more than 30 years ago however, little attention has been paid (Li et al. 2014; Yang et al. 2001) towards developing any further photo-responsive potential of polysaccharide derivatives, or preparing these light-harvesting functionalities into other more useable bio-sourced polymeric materials with high processability, for example by electrospinning.

Electrospinning, a well-established technique patented in 1934 (Formhals 1934) for manufacturing continuous nano/micro fibers and textiles by drawing polymer solutions or melts via strong electric fields between two or more electrodes, has attracted ever-increasing attention from diverse potential applications in such fields as biomedical and nanotechnological industries (Greiner and Wendorff 2007). In particular, electrospun products from natural resources including polysaccharides are promising candidates for biomedical applications such as drug delivery (Sridhar et al. 2015), tissue engineering scaffolds (Agarwal et al. 2009), and wound dressings (Rieger et al. 2013), thanks to their inherent biocompatibility and superior mechanical properties. However, electrospinning defect-free homogeneous nano/micro fibers of native polysaccharides is often challenging (Freire et al. 2011; Kulpinski 2005; Ohkawa 2008; Otsuka et al. 2017; Quan et al. 2009), due to their limited solubility in the solvents generally required for electrospinning. Modifying polysaccharides to increase their solubility in the solvents suitable for electrospinning is one of the major approaches to improve the electrospinnability of polysaccharides (Jaeger et al. 1998).

In this study, we functionalized commercially available microcrystalline cellulose with photo-responsive azobenzene groups following previous literature protocols (Arai and Udagawa 1988, 1990) with some modifications, and studied their thermal properties and kinetics of *cis/trans* photo- and thermal isomerization that were not revealed in the literature previously, although they are very important properties for the potential applications such as photo-responsive actuators. The obtained azobenzene-functionalized cellulose (Azo-Cel) was electrospun successfully for the first time from solutions of mixtures of dichloromethane (DCM) and *N,N'*-dimethylformamide (DMF) to yield well-defined nanoporous or non-porous nano/micro fibers, depending on the volatility of the solvent mixture.

## Experimental

### Materials

Avicel<sup>®</sup> PH-105 microcrystalline cellulose was purchased from FMC BioPolymer Co. and dried under vacuum at 60 °C for 24 h prior to use. 4-Phenylazobenzoyl chloride (purity: > 98.0%) was purchased from Tokyo Chemical Industry Co. and used as received. Anhydrous pyridine (purity: 99.8%) was purchased from Sigma-Aldrich Co. and used as received.

### Instruments

The <sup>1</sup>H and <sup>13</sup>C NMR spectra were recorded on a Varian Mercury 300 MHz and Varian VNMRs 500 MHz instruments, respectively. The <sup>13</sup>C Cross-polarization/Magic angle spinning (CP/MAS) experiments were performed with a Bruker Avance III 400 MHz spectrometer operated at 100.6 MHz. The specimen was packed into a zirconia specimen rotor. The spinning rate was set at 12 kHz and the cross-polarization contact time at 2 ms. A recycled delay of 2 s was inserted between each cycle. The FT-IR spectra were obtained attenuated total reflection (ATR) mode using a Bruker Vertex 70 FTIR spectrometer. Elemental Analysis was performed using a Fisons EA 1108 instrument. Thermogravimetric analysis (TGA) was performed up to 500 °C using a TA instruments TGA Q50 instrument under a nitrogen

atmosphere at a heating rate of  $10\text{ }^{\circ}\text{C min}^{-1}$ . Differential scanning calorimetry (DSC) analysis was carried out using a TA instruments DSC 2500 instrument under a nitrogen atmosphere at heating and cooling rates of  $10\text{ }^{\circ}\text{C min}^{-1}$  (scan range:  $25\text{--}150\text{ }^{\circ}\text{C}$ ). The X-ray diffraction (XRD) patterns of the powder samples were recorded on a Bruker D8 ADVANCE diffractometer. The UV-vis absorption spectra were measured in a quartz cell with 1 mm path length using a Cary 300 Bio UV-Visible spectrometer. Electrospinning of Azo-Cel was performed using Fucec Esprayer ES-2000S2A equipment. The Scanning electron microscopy (SEM) images were observed at the ICMG Platform-Grenoble using a FEI QUANTA FEG 250 microscope operating at an accelerating voltage of 2 kV.

#### Synthesis of cellulose 4-phenyl azobenzoate (Azo-Cel)

Cellulose 4-phenyl azobenzoate (Azo-Cel) was synthesized according to previously reported methods (Arai and Udagawa 1988, 1990) with minor modifications. 4-Phenylazobenzoyl chloride (2.25 g, 9.20 mmol, 1.1 equiv. to the hydroxyl group of cellulose) was dissolved in anhydrous pyridine (50 mL). The solution of 4-phenylazobenzoyl chloride was added to a suspension of Avicel<sup>®</sup> PH-105 microcrystalline cellulose (0.50 g) in anhydrous pyridine (50 mL) and stirred at  $100\text{ }^{\circ}\text{C}$  for 48 h. The reaction mixture was poured into an excess amount of ethanol and the precipitate was filtered. The residue was extracted in a Soxhlet extractor with acetone for 48 h and then dried under vacuum at  $60\text{ }^{\circ}\text{C}$  to yield a dark red colored solid product (2.13 g). The degree of substitution (DS) of the hydroxyl groups by the 4-phenylazobenzoyl groups was estimated to be 2.83 from nitrogen content in the product measured by elementary analysis according to literature (Li et al. 2014; Qin et al. 2015). Anal. calcd for  $(\text{C}_{13}\text{H}_9\text{N}_2\text{O})_n$ : C 68.70, H 4.36, N 10.68; found: C 68.57, H 4.46, N 10.52.

#### UV-Vis spectral analysis

The UV-Vis spectra of 4-phenylazobenzoyl chloride (azo dye) and Azo-Cel were measured in THF with concentrations of  $0.015\text{ g L}^{-1}$  and  $0.030\text{ g L}^{-1}$ , respectively at room temperature. The sample

solutions were irradiated with UV ( $\lambda = 365\text{ nm}$ ) and visible ( $\lambda = 460\text{ nm}$ ) light using an LED light source (10.7 mW) at a distance of ca. 10 cm from the samples for defined periods of time, followed by the spectral measurements.

#### Electrospinning

The electrospinning of Azo-Cel dissolved in mixtures of DCM and DMF with various volume ratios was performed at room temperature and humidity. The concentration of Azo-Cel was fixed at 10 wt%. A metallic electrode plate wrapped with aluminum foil was placed 15 cm away from the needle (Nordson Stainless Steel Tips 18 Gauge; inner diameter = 0.84 mm/outer diameter = 1.27 mm). High voltage (20 kV) was applied between the needle and the electrode plate while the sample solution was passed with a flow rate of (80  $\mu\text{L}/\text{min}$ ) from the needle to collect the electrospun product on the aluminum foil. The electrospun products on the aluminum foil were coated with a ca. 4 nm-thick layer of gold/palladium (Au/Pd) prior to SEM observation.

## Results and discussion

#### Functionalization of cellulose with azobenzene groups

Commercially available microcrystalline cellulose (Avicel<sup>®</sup> PH-105) was functionalized with a reversible molecular photo-switch, azobenzene, via esterification between the hydroxyl groups of cellulose and 4-(phenylazo)benzoyl chloride (azo dye) in anhydrous pyridine (Scheme 1). The product was isolated by precipitation in ethanol followed by an extraction in a Soxhlet extractor with acetone, a good solvent for the azo dye. In the IR spectrum of the product (Fig. 1), typical absorption bands of C=O ( $1723\text{ cm}^{-1}$ ) and C–O ( $1258\text{ cm}^{-1}$ ) stretching vibrations of ester groups and C=C stretching vibrations of aromatic groups ( $1603\text{ cm}^{-1}$ ) corresponding to the azobenzene moiety were observed, while a broad absorption band of the O–H stretching vibration observed around  $3300\text{ cm}^{-1}$  in the IR spectrum of the starting cellulose disappeared. In the  $^1\text{H}$  NMR spectrum of the product (Fig. 2a), a broad signal of aromatic protons (8.2–7.0 ppm) corresponding to the azobenzene

**Scheme 1** Preparation of azobenzene-functionalized cellulose (Azo-Cel) and electrospinning from its DCM/DMF solution

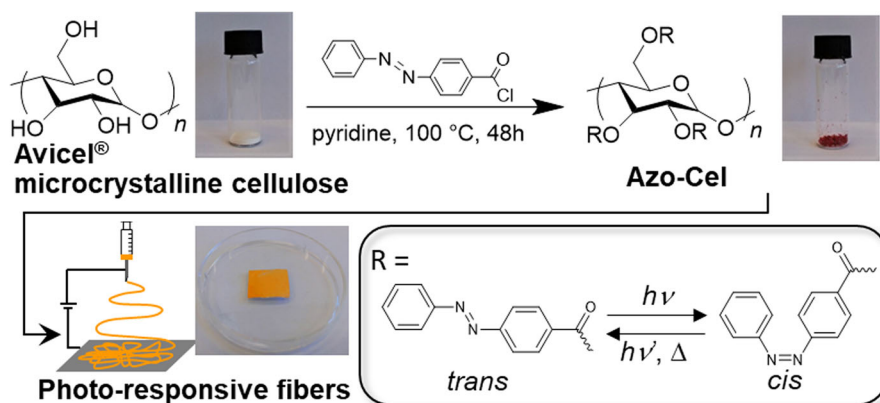
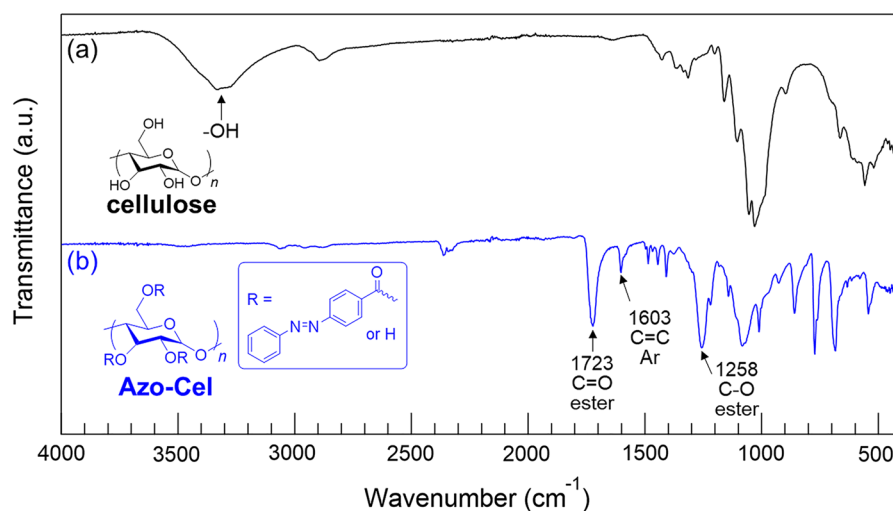


**Fig. 1** IR spectra of (a) cellulose (black) and (b) Azo-Cel (blue). (Color figure online)



moiety and a broad signal corresponding to the cellulose backbone protons (5.8–2.5 ppm) was observed. The  $^{13}\text{C}$  NMR spectrum of the product (Fig. 2b) displayed signals corresponding to carbons of each of the azobenzene, ester linkage, and cellulose groups. In addition, the  $^{13}\text{C}$  CP/MAS NMR spectrum of the product (Fig. 3b) displayed clear signals corresponding to carbon atoms of the carbonyl group around 165 ppm and of the azobenzene moiety (C–N and aromatic carbon atoms appeared respectively in 150–160 ppm and 110–135 ppm chemical shift ranges) accompanied by broadenings and upfield shifts of the signals corresponding to carbon atoms of the cellulose moiety comparing to those observed in the spectrum of cellulose (Fig. 3a). Hence, these results together strongly suggest the successful functionalization of the cellulose with the azobenzene groups. The degree of substitution (DS) of the

hydroxyl groups with the azobenzene groups was estimated to be 2.83 from the amount of nitrogen in the product determined by elemental analysis. The obtained azobenzene-functionalized cellulose (Azo-Cel) was soluble in several organic solvents that are commonly used for electrospinning such as dichloromethane (DCM), tetrahydrofuran (THF), toluene, and *N,N'*-dimethylformamide (DMF).

Figure 4 shows the X-ray diffraction (XRD) patterns of the starting cellulose and Azo-Cel. The starting cellulose displayed a typical XRD pattern of crystalline cellulose I, while no clear diffraction peaks were observed in the XRD pattern of Azo-Cel. This indicates that the crystallinity of the cellulose moiety deteriorated via the substitution of their hydroxyl groups by the azobenzene groups probably due to cleavages of hydrogen bonds in the crystal packing of cellulose. The broadenings and upfield shifts in the  $^{13}\text{C}$

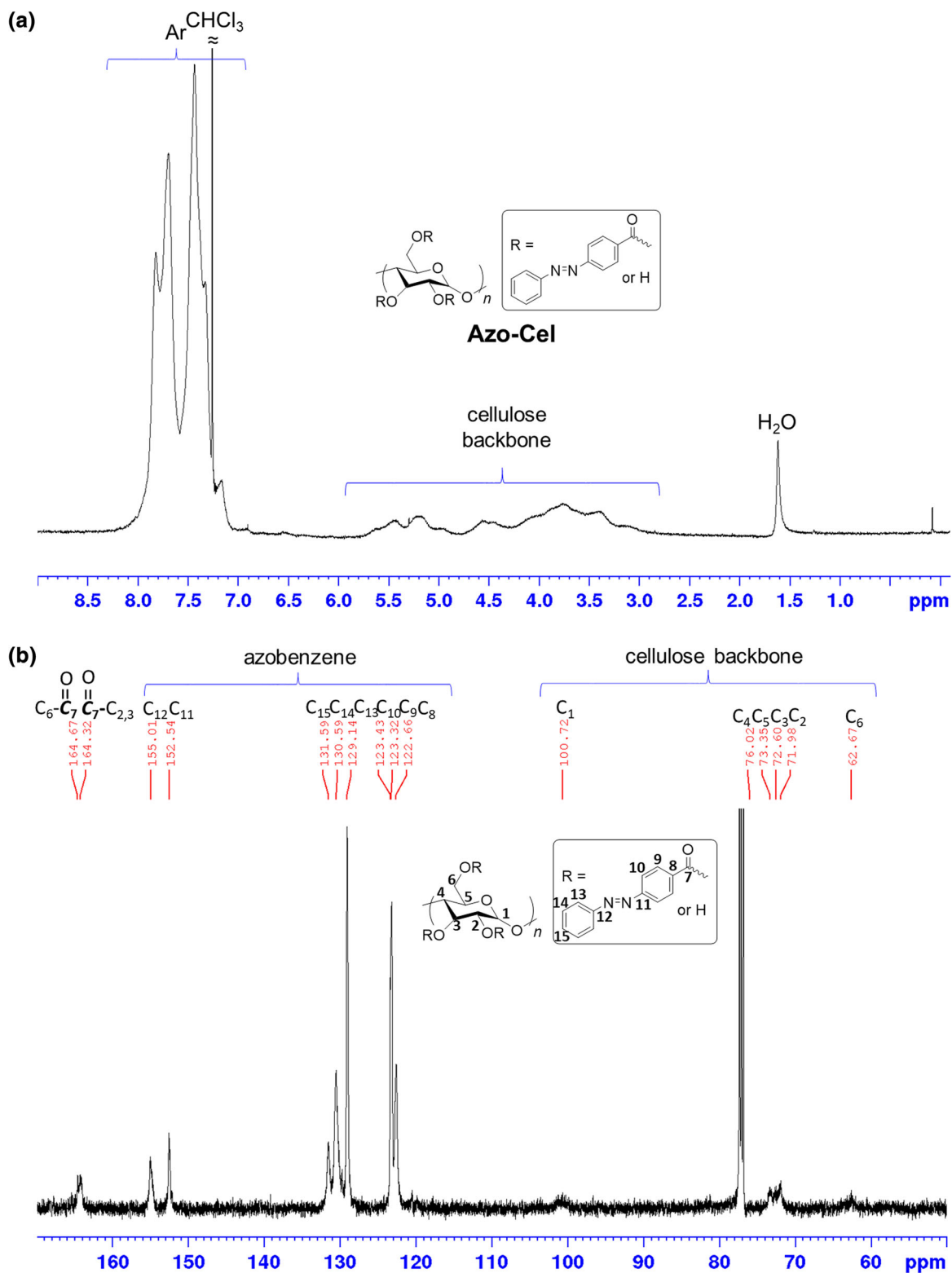


**Fig. 2** (a)  $^1\text{H}$  NMR and (b)  $^{13}\text{C}$  NMR spectra of Azo-Cel in  $\text{CDCl}_3$

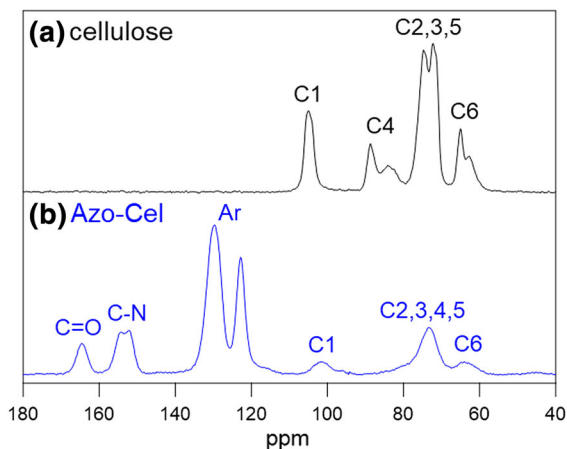


**Fig. 3**  $^{13}\text{C}$  CP/MAS NMR spectra of (a) cellulose (black) and (b) Azo-Cel (blue). (Color figure online)

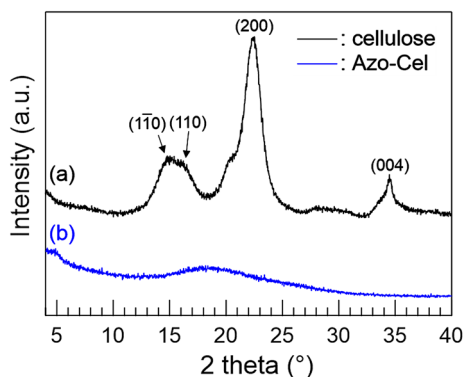


**Fig. 4** X-ray diffraction patterns of (a) cellulose (black) and (b) Azo-Cel (blue). (Color figure online)

CP/MAS NMR spectrum of Azo-Cel observed in Fig. 3b also support the amorphization of the cellulose moiety. The thermal decomposition temperature ( $T_d$ ) of the starting cellulose ( $T_d = 247^\circ\text{C}$ ) determined by thermogravimetric analysis (TGA) was increased to  $286^\circ\text{C}$  by the functionalization with azobenzene groups as shown in Fig. 5. In addition, a clear glass transition temperature ( $T_g$ ) was observed at  $172^\circ\text{C}$  in the differential scanning calorimetry (DSC) pattern of Azo-Cel, while no clear  $T_g$  was observed for the starting cellulose as shown in Fig. 6.

#### Photo-responsive properties of Azo-Cel

The UV-Vis absorption spectrum of Azo-Cel in THF showed typical absorption bands corresponding to the azobenzene group, i.e. a strong absorption band with a maximum absorption wavelength ( $\lambda_{\text{max}}$ ) at  $323\text{ nm}$

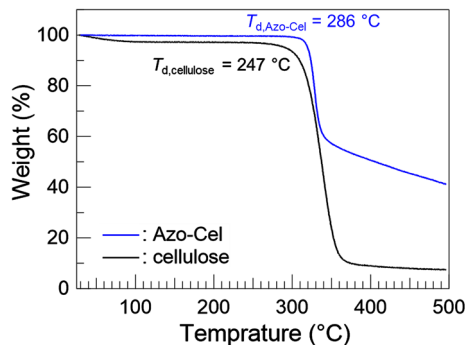


**Fig. 5** TGA traces of cellulose (black) and Azo-Cel (blue). (Color figure online)

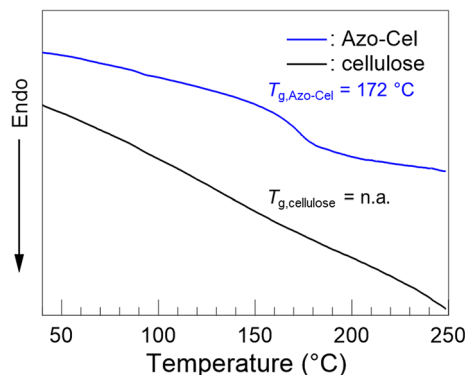


**Fig. 6** DSC traces of cellulose (black) and Azo-Cel (blue). (Color figure online)

corresponding to a  $\pi-\pi^*$  electronic transition, and a weak absorption band with  $\lambda_{\text{max}}$  at  $449\text{ nm}$  corresponding to an  $n-\pi^*$  electronic transition in the azobenzene moiety, as shown in Fig. 7a (the blue curve). These absorption bands were slightly blue-shifted in comparison with those of the un-functionalized azo dye, i.e. a strong absorption band with a  $\lambda_{\text{max}}$  at  $332\text{ nm}$  and a weak absorption band with a  $\lambda_{\text{max}}$  at  $454\text{ nm}$  (the black curve shown in Fig. 7a) upon functionalization with the cellulose. This hypsochromic effect is probably due to the fact that the azobenzene moieties in Azo-Cel are neighboring each other along the cellulose backbone, and the electron densities of the azobenzene groups are increased by a resulting  $\pi-\pi$  stacking interaction. Figure 7b shows the UV-Vis spectra of Azo-Cel dissolved in THF (the blue curve), the same solution after irradiation with UV ( $\lambda = 365\text{ nm}$ ) light (the red curve), and the same solution after irradiation with UV then visible ( $\lambda = 460\text{ nm}$ ) light (the green curve). After the irradiation with UV light, the absorbance of the band

with  $\lambda_{\max}$  at 323 nm was decreased and that of the other band with  $\lambda_{\max}$  at 449 nm was increased. This confirms the successful photoisomerization of the azobenzene moiety in Azo-Cel from the *trans*- to *cis*-isomers. After the irradiation with visible light, both absorption bands at 323 nm and 449 nm were restored to that in the original spectrum, confirming that the photoisomerization of the azobenzene moiety from the *cis*- to *trans*-isomers can cycle reversibly.

The UV-Vis absorption spectral changes of the azo dye and Azo-Cel in THF with respect to the time of the irradiation with UV light, and corresponding conversions (%) of the photoisomerization from the *trans*- to *cis*-isomers are shown in Fig. 8a, b, respectively. In a similar manner, the time-dependent UV-Vis absorption spectral changes of the azo dye and Azo-Cel solutions stored in the dark after the UV irradiation, and corresponding conversions of the thermal isomerization from the *cis*- back to *trans*- isomers are shown in Fig. 8c, d, respectively. The conversion (Conv. (%)) of photo- and thermal isomerization was determined from the peak absorbance at  $\lambda = 332$  nm for the azo dye and 323 nm for Azo-Cel according to the following Eq. (1):

$$\text{Conv.} = \frac{|A_0 - A_t|}{|A_0 - A_\infty|} \times 100(\%) \quad (1)$$

where  $A_0$ ,  $A_t$  and  $A_\infty$  are the absorbances at 0 min,  $t$  min, and equilibrium times. Here, the equilibrium time for the thermal isomerization from *cis*- to *trans*-isomers is determined as 200 min for the azo dye and 2700 min for Azo-Cel where the peak absorbances fully restored to the original absorbances before the UV irradiation.

As shown in Fig. 8a, b, the *trans-cis* photoisomerization of both the azo dye and Azo-Cel reached an

equilibrium state after irradiation with UV light for ca. 35–40 min. The kinetic profiles of their *cis-trans* thermal isomerization follow a first-order rate process, and the rate constant ( $k$ ) can be determined according to the following Eq. (2) (Smith and Abdallah 2017):

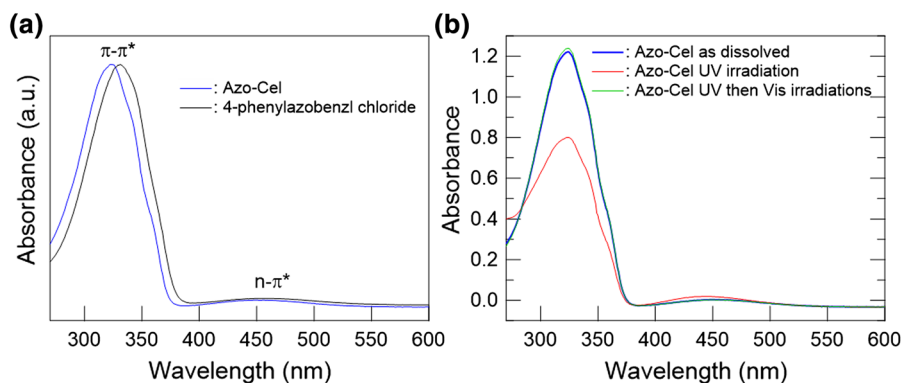
$$\ln \frac{(A_\infty - A_0)}{(A_\infty - A_t)} = kt \quad (2)$$

From the plots of  $\ln(A_\infty - A_0)/(A_\infty - A_0)$  against time as shown in Fig. 9, the  $k$  values for the azo dye and Azo-Cel were calculated to be  $1.997 \times 10^{-4} \text{ s}^{-1}$  and  $1.145 \times 10^{-5} \text{ s}^{-1}$ , respectively. This indicates that the thermal relaxation from the *cis*- back to *trans*-isomers of the azobenzene moiety in Azo-Cel is much slower than that of the azo dye, probably due to prohibitive steric hindrance derived from cellulose backbone covalently-attached with the azobenzene moiety.

#### Electrospinning of Azo-Cel

The electrospinning of the Azo-Cel solutions was investigated, towards developing light-responsive smart materials based on a strong and processable fibrous platform. For the solvents, high-volatile DCM (boiling point (bp) = 39.6 °C, vapor pressure = 47.1 kPa at 20 °C); and low-volatile DMF (bp = 153 °C, vapor pressure = 0.516 kPa at 20 °C) were mixed to adjust the volatility of the Azo-Cel solution for a stable electrospinning process, forming a cone-like shaped structure of the solution on the tip of a needle-electrode (Greiner and Wendorff 2007). The distance between the needle-electrode and a counter plate-electrode (15 cm), the applied voltage (20 kV), and the solution flow rate (80  $\mu\text{L}/\text{min}$ ) were kept at constant values. Figure 10 shows the SEM images of

**Fig. 7** The UV-Vis absorption spectra of (a) 4-(phenylazo)benzoyl chloride (black) and Azo-Cel (blue) and (b) Azo-Cel as dissolved (blue), Azo-Cel after 20 min UV ( $\lambda = 365$  nm) irradiation (red), and Azo-Cel after 20 min UV then 1 min visible light ( $\lambda = 460$  nm) irradiation (green) in THF. (Color figure online)



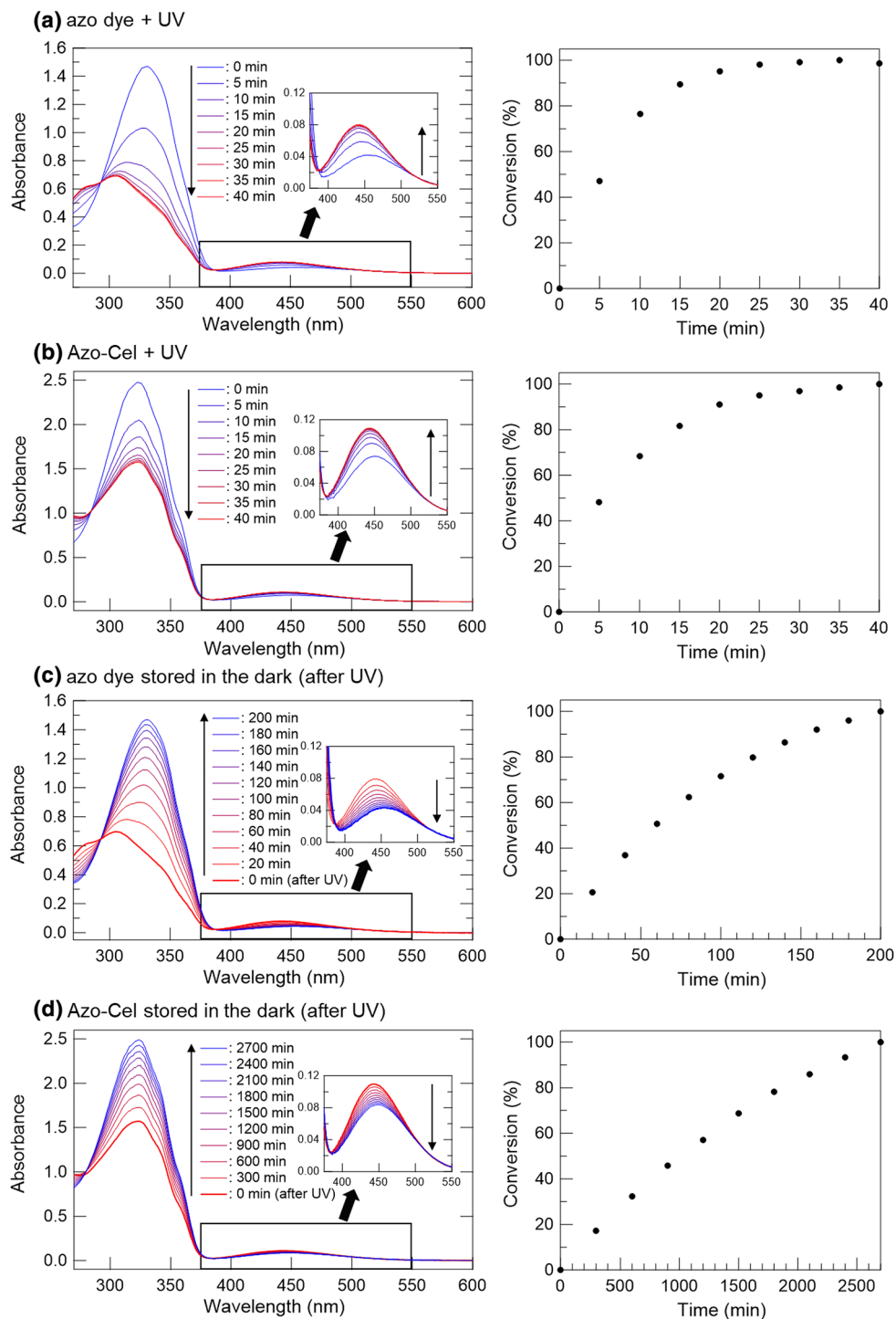


**Fig. 8** The time-dependent UV-Vis absorption spectral changes (left) and corresponding conversion (%) of the photo- and thermal isomerization as a function of time (right) of (a) 4-(phenylazo)benzoyl chloride (azo dye) and (b) Azo-Cel in THF

under UV ( $\lambda = 365$  nm) irradiation, and the same solutions of (c) the azo dye and (d) Azo-Cel stored in the dark at room temperature after UV irradiation

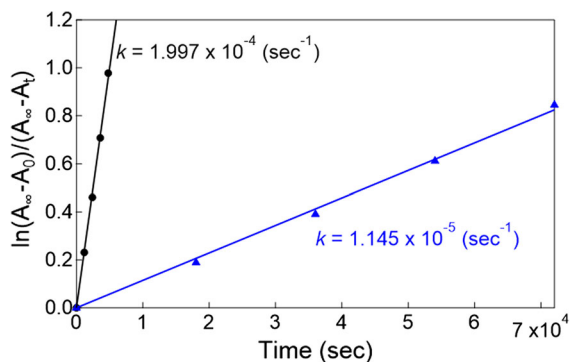


**Fig. 9** Kinetic profile and the first-order rate constant ( $k$ ) of the *cis-trans* thermal isomerization of 4-(phenylazo)benzoyl chloride (black) and Azo-Cel (blue) in THF. (Color figure online)

the electrospun products obtained from the Azo-Cel solutions in the mixtures of DCM and DMF with different volume ratios. Here, it should be noted that the Azo-Cel solution in DCM 100% was not electrospinnable stably because the solution was too highly volatile and quickly stuck within the needle in a few seconds by natural evaporation during the electrospinning process. By mixing 10 vol% of DMF with DCM (DCM:DMF = 9:1 (v/v)), the Azo-Cel solution became less volatile and electrospinnable more stably. The electrospun product from this solution showed a good fibrous structure (Fig. 10a–c) with the averaged diameter ( $D$ ) of 2.61  $\mu\text{m}$  determined by a statistical analysis for 50 randomly selected fibers from the SEM image (Fig. 10a) using ImageJ open-source software. Interestingly, the high-magnified (magnification: 20,000  $\times$ ) SEM image of the fibers (Fig. 10c) showed a nanoporous structure. Diameters of these pores ranges from ca. 5 to 50 nm as observed in the high-resolution SEM image (Fig. S1: see Supplementary data). By increasing the volume ratio of DMF up to 25 vol% (DCM:DMF = 7.5:2.5 (v/v)), the Azo-Cel solution displayed the most stable electrospinnability within the conditions investigated in this study. The electrospun product from this solution showed more homogeneous and thinner fibers (Fig. 10d–f) with  $D = 760$  nm determined from the SEM image (Fig. 10e) than that from the 10 vol% of DMF solution. The highly-magnified SEM image of these fibers showed a smooth surface morphology (Fig. 10f) unlike the nanoporous fibers obtained from the

10 vol% DMF solution (Figs. 10c and S1). This can be explained by the difference of the vapor pressure of the solvents. Because the Azo-Cel solution in 10 vol% of DMF has higher vapor pressure than the solution in 25 vol% of DMF, the solvent evaporates more rapidly from the 10 vol% DMF solution than from the 25 vol% DMF solution. Such a rapid solvent evaporation forms the nanoporous structure within the fibers during the electrospinning process. Other hypotheses for the creation of porous structures were reported in literature such as the traces of evaporations of water droplets on the surface of the fibers (Casper et al. 2004) or a phase separation into polymer-rich and polymer-poor regions (Megelski et al. 2002) that occurs upon evaporation of the solvents. By further increasing the volume ratio of DMF to DCM, the electrospun products showed a spherical bead-like structure coexisting with the fibrous structure when the ratio of DMF was 50 vol% (Fig. 10g–i). From the 75 vol% DMF solution, irregular-shaped beads linked with extremely thin fibers were electrospun (Fig. 10j–l). Only random spheres but no fibers were obtained by electrospinning from the 100% DMF solution (Fig. 10m–o). These results clearly indicate that the morphology of the electrospun fibers of Azo-Cel can be controlled simply by adjusting the volatility of the solvent within the conditions investigated in this study. Notably, the nanoporous structure of the nanofibers may well be an added advantage of interest when the electrospun fibrous materials are used for potential applications such as nanofiltration membranes thanks to their large surface-area-to-volume ratio.

The azobenzene moiety in Azo-Cel showed *cis/trans* isomerization in response to photo- and thermal stimuli as discussed in the previous section. Such a modest geometric variation that occurs in an individual azobenzene molecule can be amplified cooperatively with the neighboring azobenzene groups on the cellulosic backbones, and their fibrous assemblies where the azobenzene molecules form clusters, to induce large-scale changes in physical properties such as dipole moment, polarity, shape *etc.* of the Azo-Cel fibrous materials. These various physical aspects are under investigation and will be the subject of a forthcoming paper.

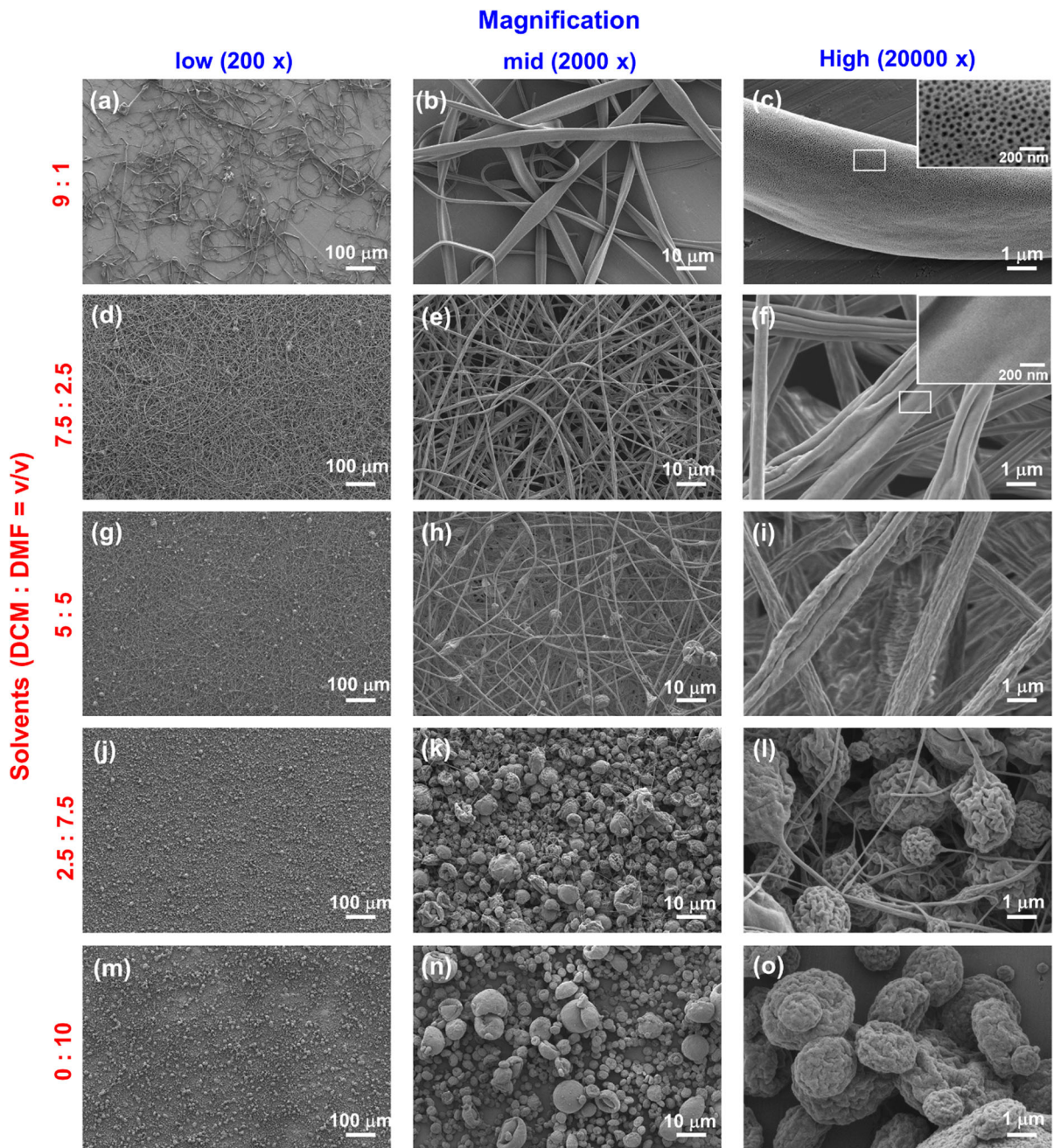


**Fig. 10** SEM images with low (left column), mid (center column), and high (right column) magnifications of the electrospun Azo-Cel from their solutions of mixtures of DCM and DMF with volume ratios of DCM:DMF = 9:1 (top line: a–

c), 7.5:2.5 (upper middle line: d–f), 5:5 (middle line: g–i), 2.5:7.5 (lower middle line: j–l), and 0:10 (bottom line: m–o). Inserts in c and f are their digitally zoomed images

## Conclusion

In summary, we have demonstrated the successful functionalization of commercially available

microcrystalline cellulose with photo-responsive azobenzene moieties to yield Azo-Cel, the *cis/trans* isomerization of the azobenzene moiety in Azo-Cel in response to photo- and thermal stimuli, and the

fabrication of the nanoporous and non-porous nano/micro fibrous materials by electrospinning of Azo-Cel solutions in the mixtures of DCM and DMF to control the volatility of the solutions. These novel cellulose-based robust fibrous materials, with light-reversible functional groups, opens up the potential of natural resources that can be derived from biomass towards state-of-the-art stimuli-responsive materials for applications such as photo-responsive actuators and nanofiltration membranes.

**Acknowledgments** This study was financially supported by the Natural Sciences and Engineering Research Council of Canada (NSERC), the French National Center for Scientific Research (CNRS), PolyNat Carnot Institute and LabEx Tec21. I.O. is grateful for a grant “Explo’RA PRO” (Contract No 149739) from the French Rhône-Alpes region and the CNRS which supported his sabbatical research leave in Montreal. The authors acknowledge E. Nadezhina of Univ. de Montréal for the elemental analysis, Y. Ogawa of CERMAV for the  $^{13}\text{C}$  CP/MAS NMR spectral analysis, and C. Lancelon-Pin and R. Borsali of CERMAV for the SEM observation at the ICMG Platform-Grenoble. The authors also thank the assistance of T. Borchers and V. Chang of McGill Univ. for the UV-Vis spectral analysis.

## References

- Agarwal S, Wendorff JH, Greiner A (2009) Progress in the field of electrospinning for tissue engineering applications. *Adv Mater* 21:3343–3351. <https://doi.org/10.1002/adma.200803092>
- Arai K, Udagawa H (1988) Application of photoresponsive groups-containing cellulose as an adsorbent for thin layer chromatography. *Die Makromol Chem Rapid Commun* 9:797–800. <https://doi.org/10.1002/marc.1988.030091203>
- Arai K, Udagawa H (1990) Influence of DP of cellulose backbone on liquid crystalline phase of cellulose p-phenylazobenzoate. *Sen’i Gakkaishi* 46:491–495. [https://doi.org/10.2115/fiber.46.11\\_491](https://doi.org/10.2115/fiber.46.11_491)
- Casper CL, Stephens JS, Tassi NG, Chase DB, Rabolt JF (2004) Controlling surface morphology of electrospun polystyrene fibers: effect of humidity and molecular weight in the electrospinning process. *Macromolecules* 37:573–578. <https://doi.org/10.1021/ma0351975>
- Chauhan P et al (2014) A nanocellulose–dye conjugate for multi-format optical pH-sensing. *Chem Commun* 50:9493–9496. <https://doi.org/10.1039/C4CC02983F>
- Dong S, Roman M (2007) Fluorescently labeled cellulose nanocrystals for bioimaging applications. *J Am Chem Soc* 129:13810–13811. <https://doi.org/10.1021/ja0761961>
- Ercole F, Davis TP, Evans RA (2010) Photo-responsive systems and biomaterials: photochromic polymers, light-triggered self-assembly, surface modification, fluorescence modulation and beyond. *Polym Chem* 1:37–54. <https://doi.org/10.1039/b9py00300b>
- Formhals A (1934) Process and apparatus for preparing artificial threads. US1975504A
- Freire MG, Teles ARR, Ferreira RAS, Carlos LD, Lopes-da-Silva JA, Coutinho JAP (2011) Electrospun nanosized cellulose fibers using ionic liquids at room temperature. *Green Chem* 13:3173–3180. <https://doi.org/10.1039/c1gc15930e>
- Gorgieva S, Vogrinčič R, Kokol V (2015) Polydispersity and assembling phenomena of native and reactive dye-labelled nanocellulose. *Cellulose* 22:3541–3558. <https://doi.org/10.1007/s10570-015-0755-3>
- Greiner A, Wendorff JH (2007) Electrospinning: a fascinating method for the preparation of ultrathin fibers. *Angew Chem Int Ed Engl* 46:5670–5703. <https://doi.org/10.1002/anie.200604646>
- Harada A, Takashima Y, Nakahata M (2014) Supramolecular polymeric materials via cyclodextrin-guest interactions. *Acc Chem Res* 47:2128–2140. <https://doi.org/10.1021/ar500109h>
- Huang J-L, Li C-J, Gray DG (2013) Cellulose nanocrystals incorporating fluorescent methylcoumarin groups. *ACS Sustain Chem Eng* 1:1160–1164. <https://doi.org/10.1021/sc400074e>
- Ikeda T, Mamiya J, Yu Y (2007) Photomechanics of liquid-crystalline elastomers and other polymers. *Angew Chem Int Ed Engl* 46:506–528. <https://doi.org/10.1002/anie.200602372>
- Ikejiri S, Takashima Y, Osaki M, Yamaguchi H, Harada A (2018) Solvent-Free photoresponsive artificial muscles rapidly driven by molecular machines. *J Am Chem Soc* 140:17308–17315. <https://doi.org/10.1021/jacs.8b11351>
- Jaeger R, Bergshoeff MM, Battle CMI, Schönherr H, Julius Vancso G (1998) Electrospinning of ultra-thin polymer fibers. *Macromol Symp* 127:141–150. <https://doi.org/10.1002/masy.19981270119>
- Klemm D, Heublein B, Fink HP, Bohn A (2005) Cellulose: fascinating biopolymer and sustainable raw material. *Angew Chem Int Ed Engl* 44:3358–3393. <https://doi.org/10.1002/anie.200460587>
- Kulpinski P (2005) Cellulose nanofibers prepared by the N-methylmorpholine-N-oxide method. *J Appl Polym Sci* 98:1855–1859. <https://doi.org/10.1002/app.22123>
- Li Z, Zhang D, Weng J, Chen B, Liu H (2014) Synthesis and characterization of photochromic azobenzene cellulose ethers. *Carbohydr Polym* 99:748–754. <https://doi.org/10.1016/j.carbpol.2013.08.093>
- Megelski S, Stephens JS, Chase DB, Rabolt JF (2002) Micro- and nanostructured surface morphology on electrospun polymer fibers. *Macromolecules* 35:8456–8466. <https://doi.org/10.1021/ma020444a>
- Nielsen LJ, Eyley S, Thielemans W, Aylott JW (2010) Dual fluorescent labelling of cellulose nanocrystals for pH sensing. *Chem Commun* 46:8929–8931. <https://doi.org/10.1039/C0CC03470C>
- Ohkawa K (2008) Electrospinning of natural and bio-related polymeric materials. *Fiber* 64:36–44. <https://doi.org/10.2115/fiber.64.36>
- Okamoto Y, Sakamoto H, Hatada K, Irie M (1986) Resolution of enantiomers by HPLC on cellulose trans- and cis-tris (4-phenylazophenylcarbamate). *Chem Lett* 15:983–986. <https://doi.org/10.1246/cl.1986.983>

- Otsuka I, Njinang CN, Borsali R (2017) Simple fabrication of cellulose nanofibers via electrospinning of dissolving pulp and tunicate. *Cellulose* 24:3281–3288. <https://doi.org/10.1007/s10570-017-1360-4>
- Pei Z, Yang Y, Chen Q, Terentjev EM, Wei Y, Ji Y (2014) Mouldable liquid-crystalline elastomer actuators with exchangeable covalent bonds. *Nat Mater* 13:36–41. <https://doi.org/10.1038/nmat3812>
- Qin W, Li Z, Li J, Zhang L, Liu R, Liu H (2015) Synthesis and characterization of azobenzene hydroxypropyl cellulose with photochromic and thermotropic liquid crystal properties. *Cellulose* 22:203–214. <https://doi.org/10.1007/s10570-014-0479-9>
- Quan S-L, Kang S-G, Chin I-J (2009) Characterization of cellulose fibers electrospun using ionic liquid. *Cellulose* 17:223–230. <https://doi.org/10.1007/s10570-009-9386-x>
- Rieger KA, Birch NP, Schiffman JD (2013) Designing electrospun nanofiber mats to promote wound healing—a review. *J Mater Chem B* 1:4531–4541. <https://doi.org/10.1039/c3tb20795a>
- Smith S, Abdallah FB (2017) The kinetics of the cis-to-trans thermal isomerization of 4-anilino-4'-nitroazobenzene are highly influenced by solvent polarity. *J Thermodyn Catal* 08:1–6. <https://doi.org/10.4172/2157-7544.1000181>
- Sridhar R, Lakshminarayanan R, Madhaiyan K, Amutha Barathi V, Lim KHC, Ramakrishna S (2015) Electrospayed nanoparticles and electrospun nanofibers based on natural materials: applications in tissue regeneration, drug delivery and pharmaceuticals. *Chem Soc Rev* 44:790–814. <https://doi.org/10.1039/C4CS00226A>
- Yang S, Jacob MM, Li L, Cholli AL, Kumar J, Tripathy SK (2001) Synthesis and characterization of novel azobenzene-modified polymers: azocellulose. *Macromolecules* 34:9193–9196. <https://doi.org/10.1021/ma010931a>
- Zeng H, Wani OM, Wasylczyk P, Priimagi A (2018) Light-driven, caterpillar-inspired miniature inching robot. *Macromol Rapid Commun* 39:1700224. <https://doi.org/10.1002/marc.201700224>

**Publisher's Note** Springer Nature remains neutral with regard to jurisdictional claims in published maps and institutional affiliations.